SUPPLEMENTAL MATERIAL

Supplemental Figure 1: Fluo2-loaded islets and GLP-1 dose responses.

Supplemental Figure 2: Glucose- and GLP-1R-dependency of islet Ca^{2+} responses to incretin.

Supplemental Figure 3: Gap junction (GJ) blockade doesn't affect cell responses to depolarising stimuli.

Supplemental Figure 4: Silencing of gap junction (GJ) expression impairs coordinated cell responses to GLP-1.

Supplemental Figure 5: Palmitate reduces gap junction (GJ) protein expression.

Supplemental Figure 6: Palmitate impairs glucose-stimulated insulin secretion.

Supplemental Figure 7: Representative Ca^{2+} traces of control-, palmitate- and palmitate+H89-treated islets.

Supplemental Figure 8: Inhibition of PKA does not acutely affect Ca^{2+}-responses to incretin.

Supplemental Figure 9: Inter-individual variability does not alter deleterious effects of palmitate on coordinated cell-cell activity.

Supplemental Figure 10: *In vivo* validation of exendin4-FITC binding.

Supplemental Figure 11: Ca^{2+}-responses to carbachol and tolbutamide are unaffected by gap junction (GJ) blockade.

Supplemental Figure 12: Glucose tolerance, Cx36 expression and cell viability in high fat diet (HFD)-fed mice.

Supplemental Figure 13: Incubation of mouse islets with palmitate does not alter the fold-change of GLP-stimulated insulin secretion.

Supplemental Figure 14: Schematic depicting proposed mechanisms underlying GLP-1 effects on coordinated cell-cell activity.

Supplemental Table 1: Summary of donor age, gender, BMI and origin.

Supplemental Table 2: Primer sequences used for quantitative real-time polymerase chain reaction studies (qPCR).

Supplemental Movie 1: Timelapse recording of calcium responses to GLP-1 in a human islet.

Supplemental Movie 2: Timelapse recording of GLP-1-stimulated insulin release in BGA-treated islets using the Zn^{2+}-probe ZIMIR.

Supplemental Movie 3: Timelapse recording of GLP-1-stimulated insulin release in AGA-treated islets using the Zn^{2+}-probe ZIMIR.

Supplemental Movie 4: Timelapse recording of calcium responses to glucose and GLP-1 in a normal diet mouse islet.

Supplemental Movie 5: Timelapse recording of calcium responses to glucose and GLP-1 in a high fat diet mouse islet.

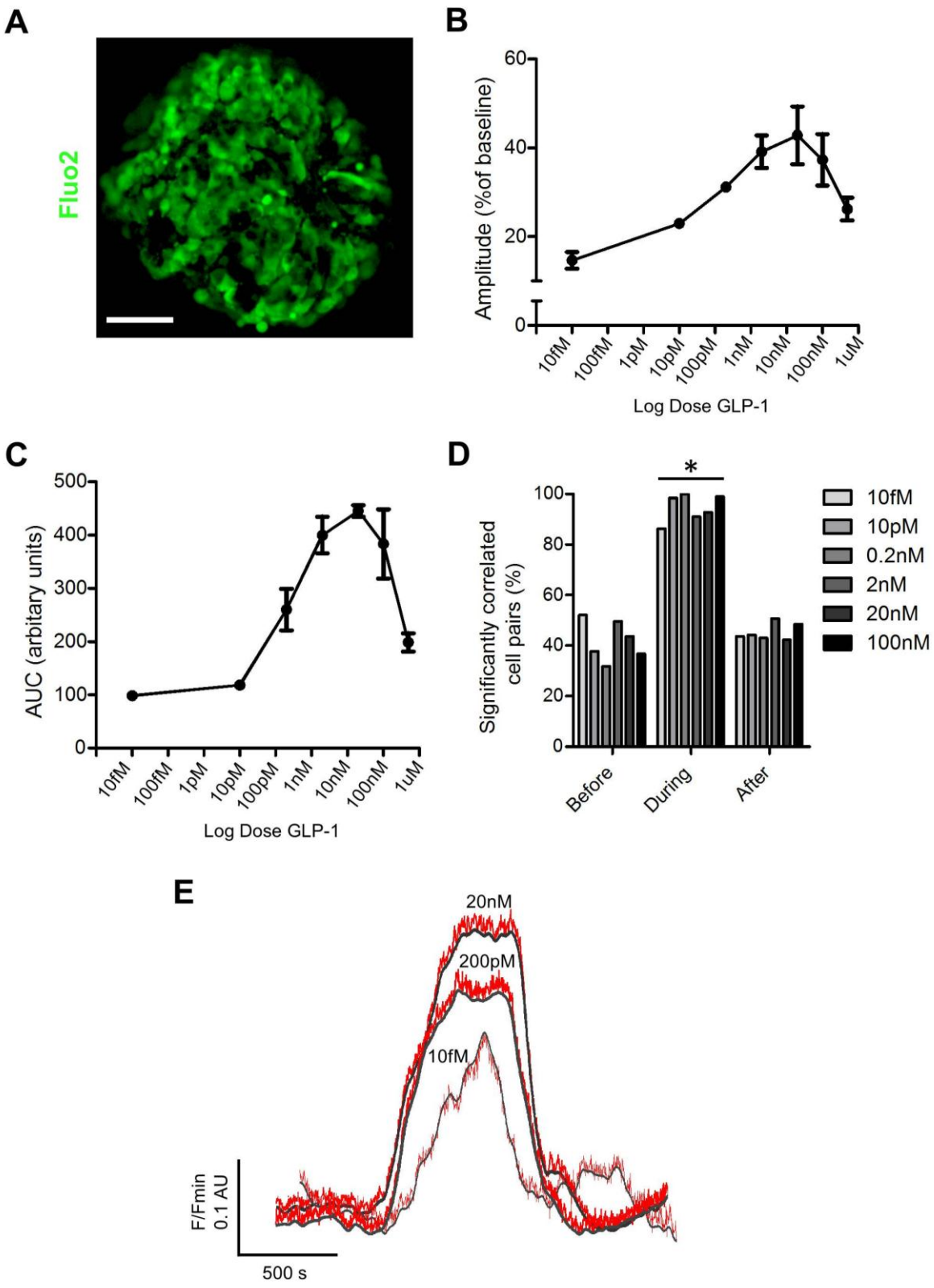

Supplemental Figure 1: Fluo2-loaded islets and GLP-1 dose responses. **(A)** Optical section through a fluo2-loaded human islet (scale bar, 40 µm). **(B)** Dose-response (log scale) demonstrates maximal amplitude of Ca^{2+} rises following stimulation with 20 nM GLP-1 (*n*=3 recordings). **(C)** As for (B) but area under the curve (AUC). **(D)** GLP-1 10 fM-100 nM stimulates identical and significant increases in correlated cell-cell behaviour (*P<0.05 *versus* Before GLP-1 application, two-way ANOVA; *n*=3 recordings). **(E)** Representative Ca^{2+}-responses to 10 fM, 200 pM and 20 nM GLP-1. Values represent mean ± SEM.

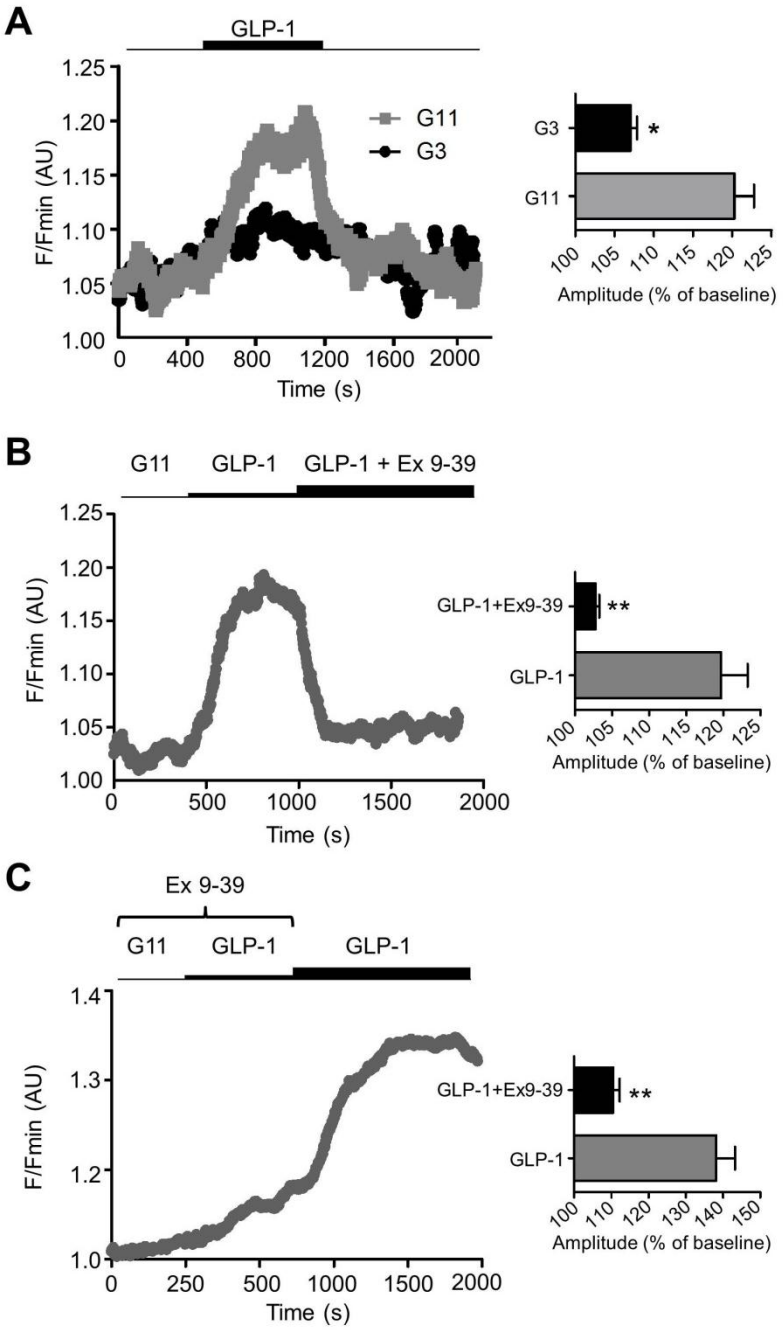

Supplemental Figure 2: Glucose- and GLP-1R-dependency of islet Ca^{2+}-responses to incretin. **(A)** Ca^{2+}-responses to GLP-1 are present at 11 mM but not 3 mM glucose (mean traces, left panel) (*P<0.05 *versus* G3, Mann-Whitney U-test; *n*=4-5 recordings from three donors). **(B)** GLP-1-induced increases in $[Ca^{2+}]_i$ are abrogated by post-application of 100 nM exendin 9-39 (Ex 9-39), a competitive GLP-1R antagonist (mean traces, left panel) (**P<0.01 *versus* GLP-1, Mann-Whitney U-test; *n*=5 recordings from three donors). **(C)** Pre-application of 100 nM Ex 9-39 reversibly prevents GLP-1 from evoking Ca^{2+}-rises (mean traces, left panel) (**P<0.01 *versus* GLP-1, Mann-Whitney U-test; *n*=3 recordings). Values represent mean ± SEM.

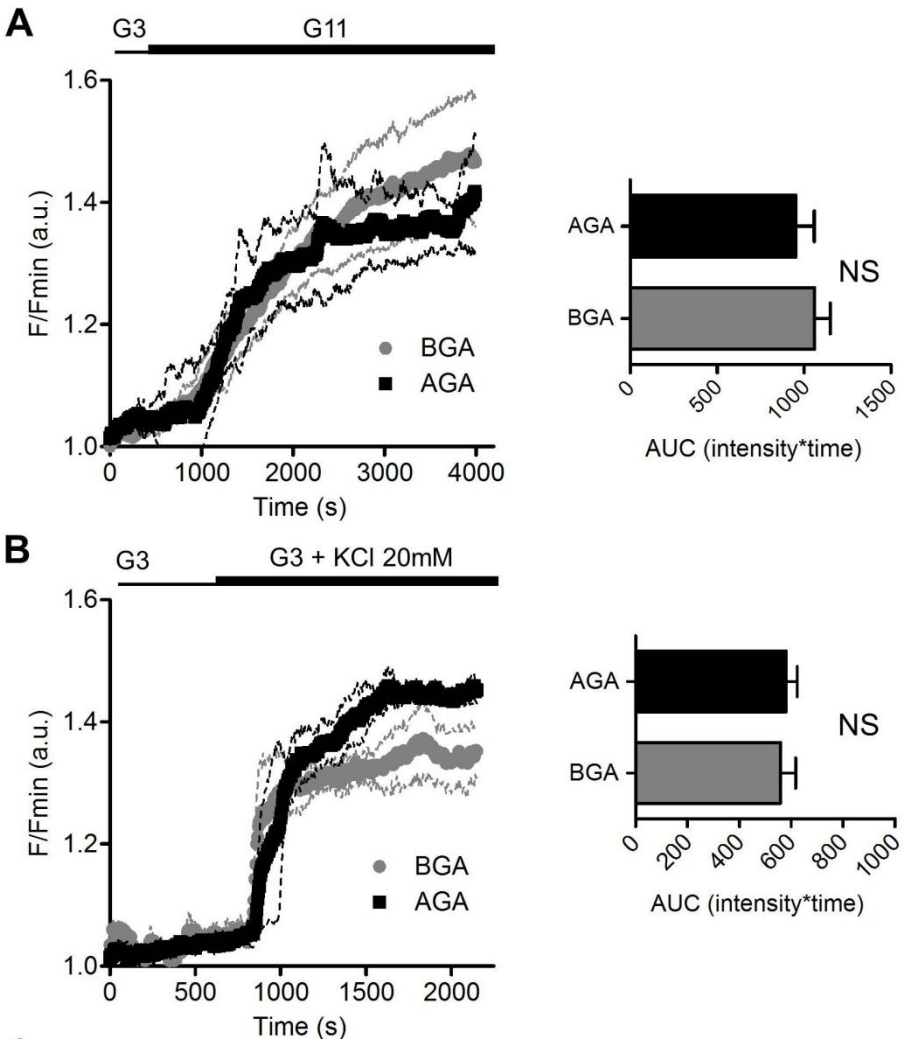

Supplemental Figure 3: Gap junction **(**GJ) blockade does not affect cell responses to depolarizing stimuli. **(A)** The GJ-blocker 18-α glycerrhithinic acid (AGA) does not alter Ca^{2+} responses to 11 mM glucose (G11) *versus* its inactive analog, β-glycerrhizic acid (BGA) (NS, non-significant *versus* control (Con); Mann-Whitney U-test) (mean traces ± standard deviation (S.D); left panel; *n*=3 recordings). **(B)** As for **(A)** but following application of the generic depolarizing stimulus, potassium chloride (KCl) (*n*=3 recordings). Unless otherwise stated, values represent mean ± SEM.

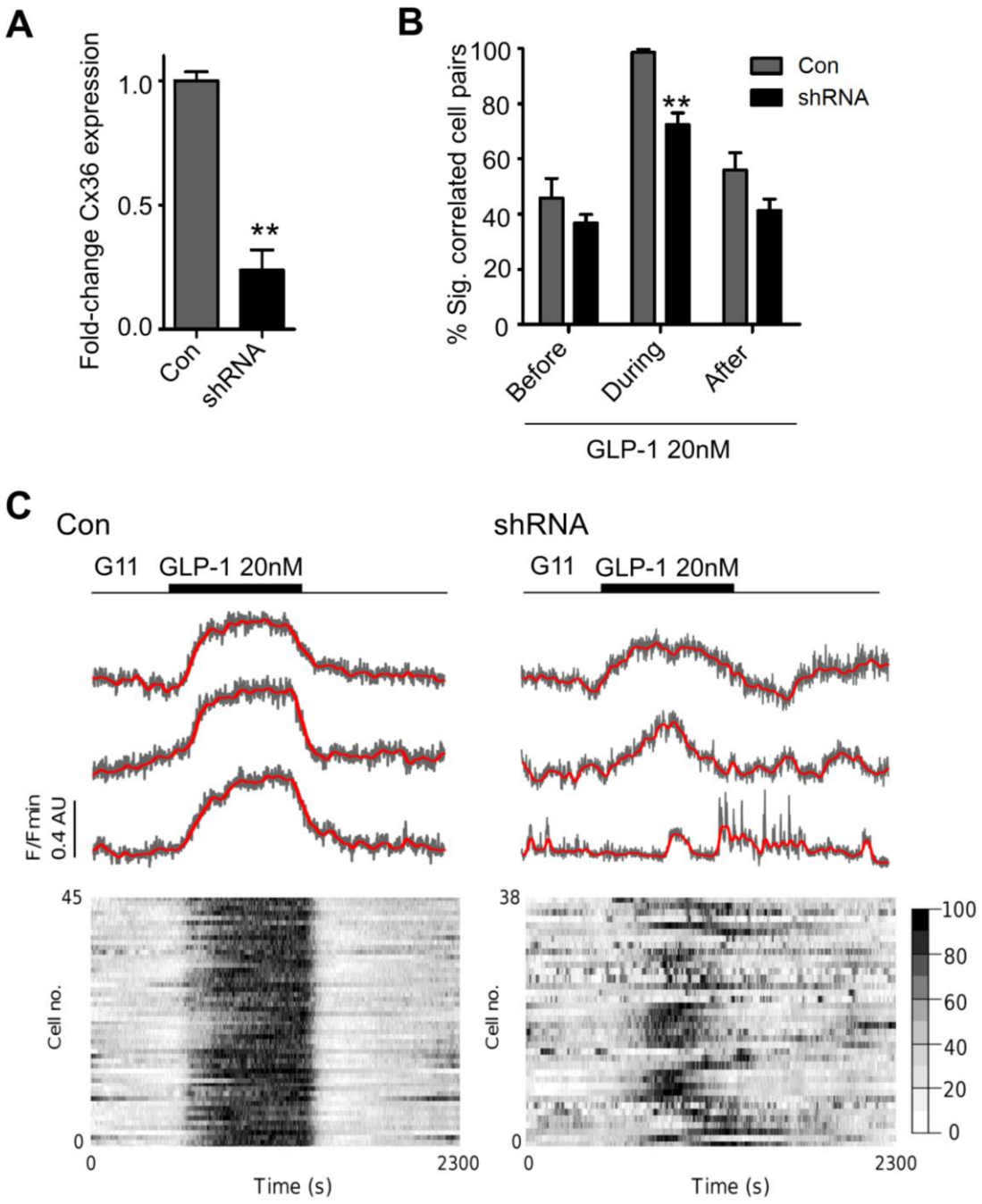

Supplemental Figure 4: Silencing of gap junction (GJ) expression impairs coordinated cell responses to GLP-1. **(A)** Cx36 short hairpin RNA (shRNA) reduces transcript levels in human islet cells (**P<0.01 *versus* control (Con), Student's t-test) (*n*=3 donors). **(B)** Cx36 knockdown impairs coordinated cell responses to GLP-1 (**P<0.01, two-way ANOVA) (*n*=10 islets from three donors). **(C)** Representative Ca^{2+}-traces from control (Con)- and shRNA-treated islets. Top panel: red, smoothed; grey, raw. Bottom panel: heatmap depicting min-max for each cell as a 100-bit color ramp.

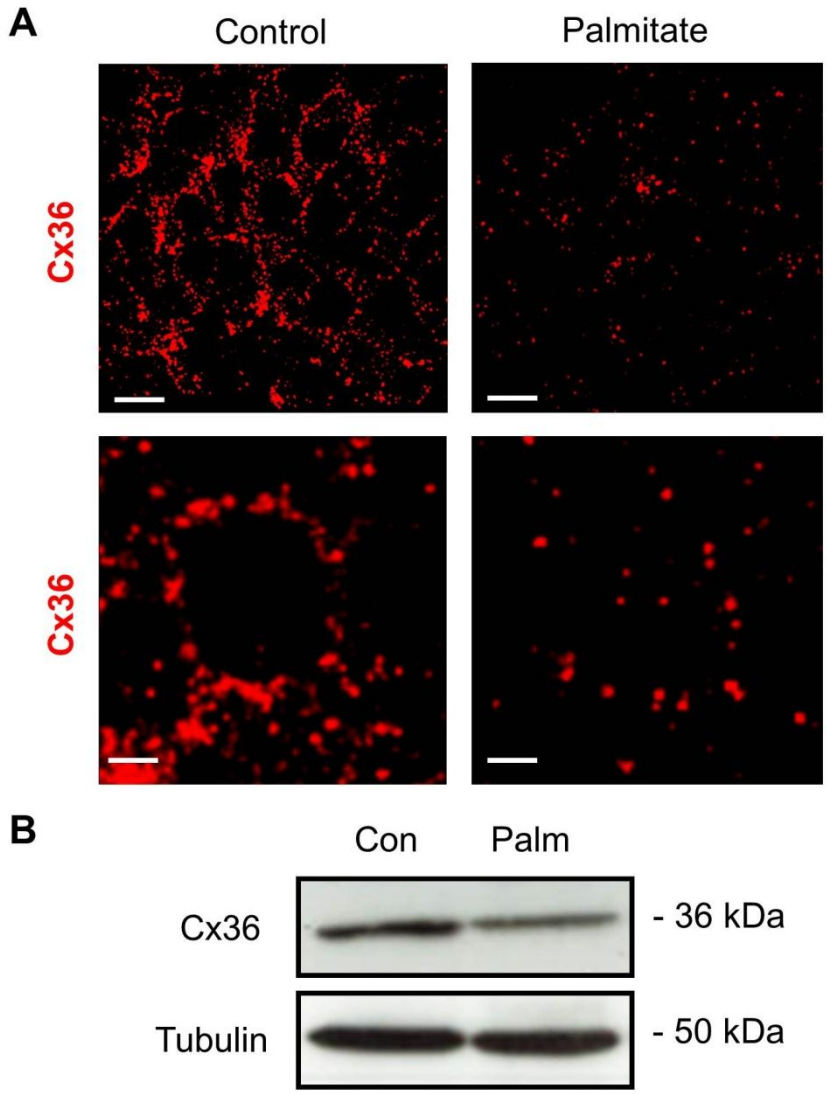

Supplemental Figure 5: Palmitate reduces gap junction (GJ) protein expression. **(A)** High resolution images of immunostained human islets reveals a decrease in connexin 36 (Cx36) immunopositivity following exposure to palmitate (magnified images; bottom panel; scale, 10 µm top and 5µm bottom). **(B)** Western (immuno-) blotting using specific antibodies against Cx36 confirms the results from **(A).** A representative blot is shown (*n*=3 blots).

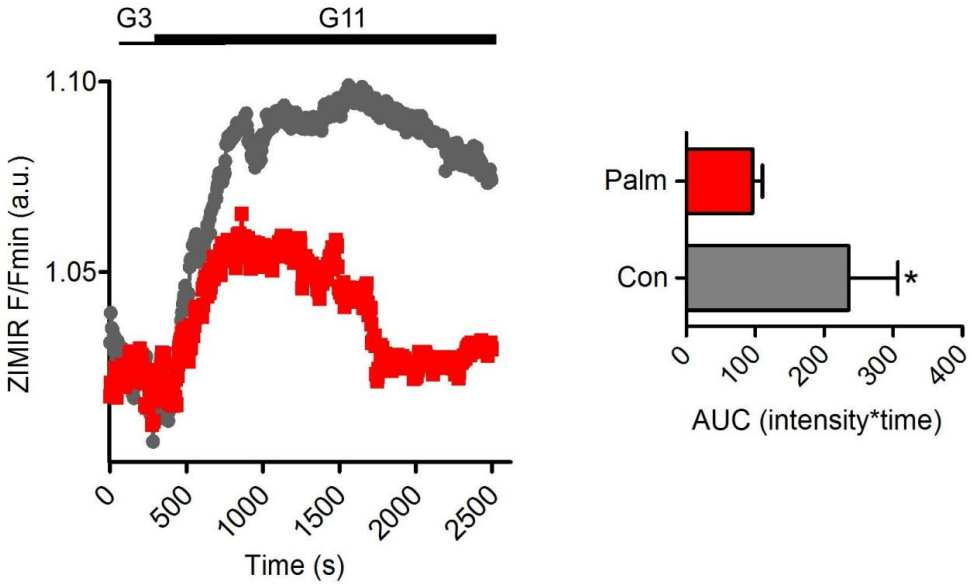

Supplemental Figure 6: Palmitate impairs glucose-stimulated insulin secretion. 72 h exposure to palmitate (Palm) alters the kinetics of 11 mM glucose (G11)-stimulated insulin secretion *versus* control (Con) islets (left). Bar graph displays the mean area under the curve (AUC) (right panel) (*P<0.05 *versus* control (Con); student's t-test; *n*=5 recordings). Values represent mean ± SEM.

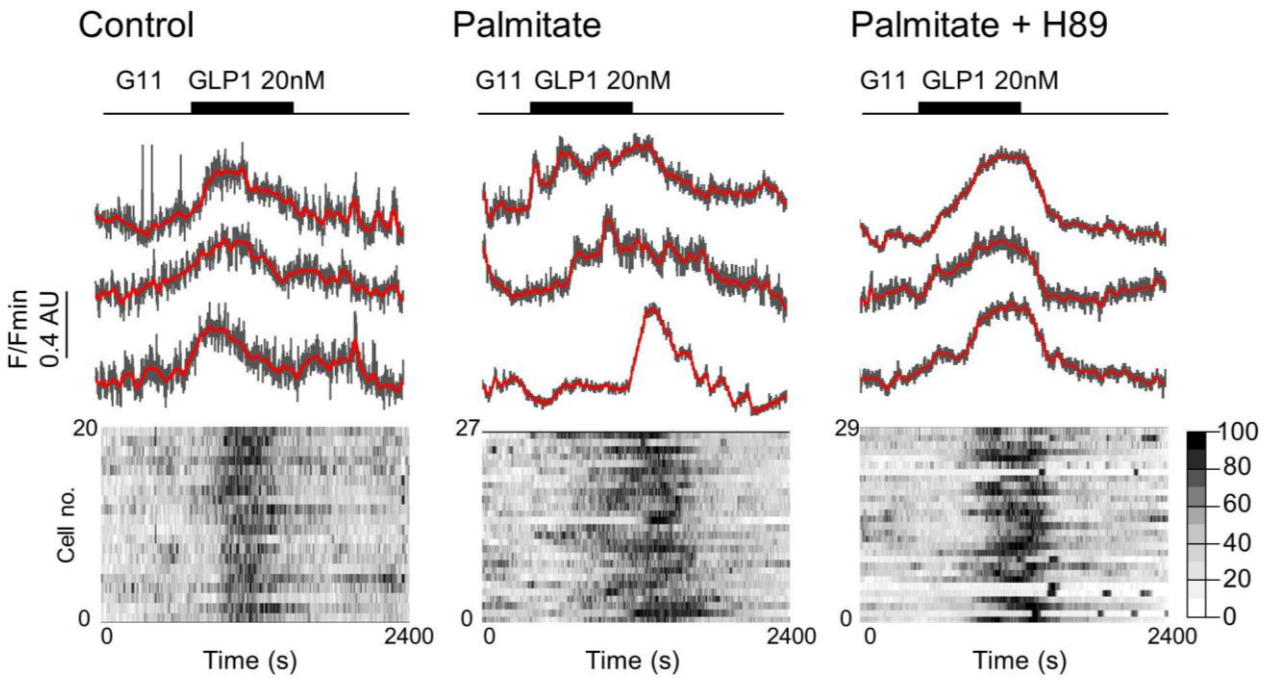

Supplemental Figure 7: Representative Ca^{2+} traces of control, palmitate and palmitate + H89 treated islets. Top panel: representative Ca^{2+} traces; red, smoothed; grey, raw. Bottom panel: heatmap depicting min-max for each cell as a 100-bit color ramp.

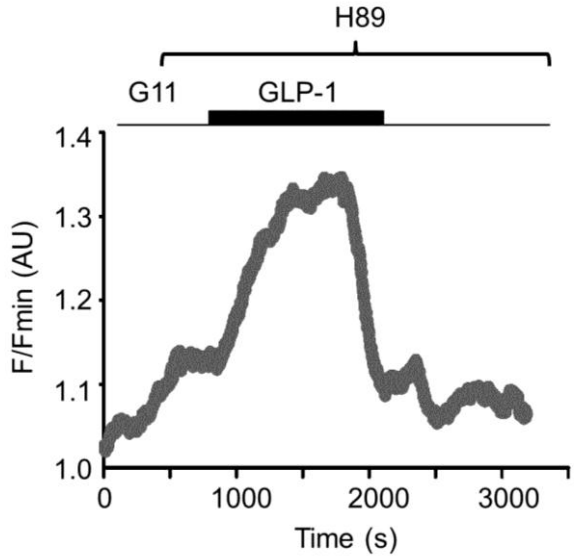

Supplemental Figure 8: Inhibition of PKA does not acutely affect Ca^{2+}-responses to incretin (mean trace of *n*=5 recordings).

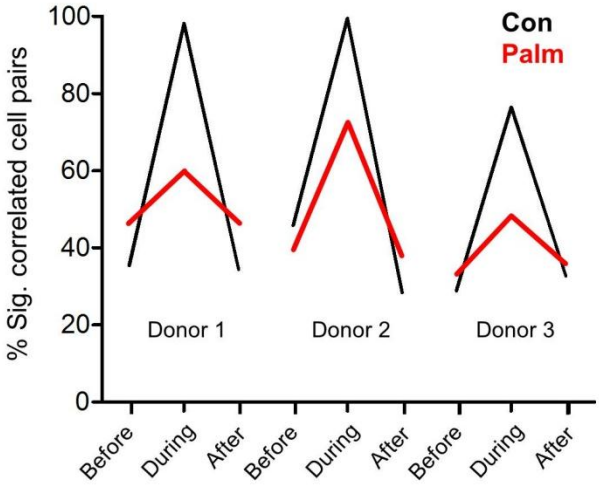

Supplemental Figure 9: Inter-individual variability does not alter deleterious effects of palmitate on coordinated cell-cell activity. Before-during-after plot demonstrates reduction in mean % significantly correlated cell pairs in palmitate- (Palm) *versus* control- (Con) treated islets obtained from three individual donors**.** Donors correspond to the isolations of 14th May, 16th May and 4th June 2012, see Supplemental Table 1.

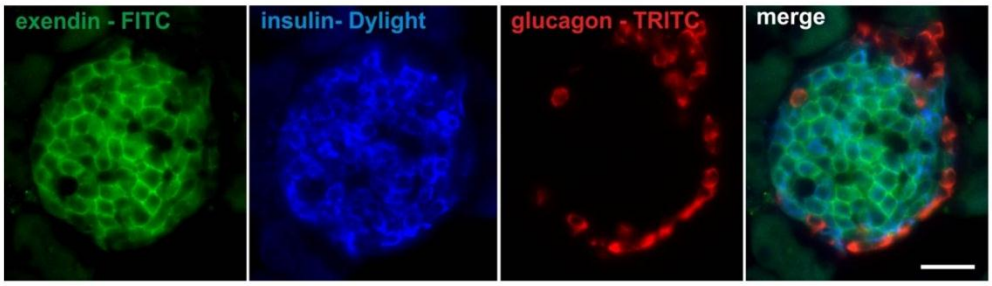

Supplemental Figure 10: *In vivo* validation of exendin4-FITC binding. One hour after the *in vivo* administration of exendin4-FITC to mice, a section of pancreas was immunostained for FITC (green), insulin (blue) and glucagon (red). In all islets, exendin4 was easily detected at the surface of virtually all beta- but less so in alpha-cells (scale bar, 40 μm).

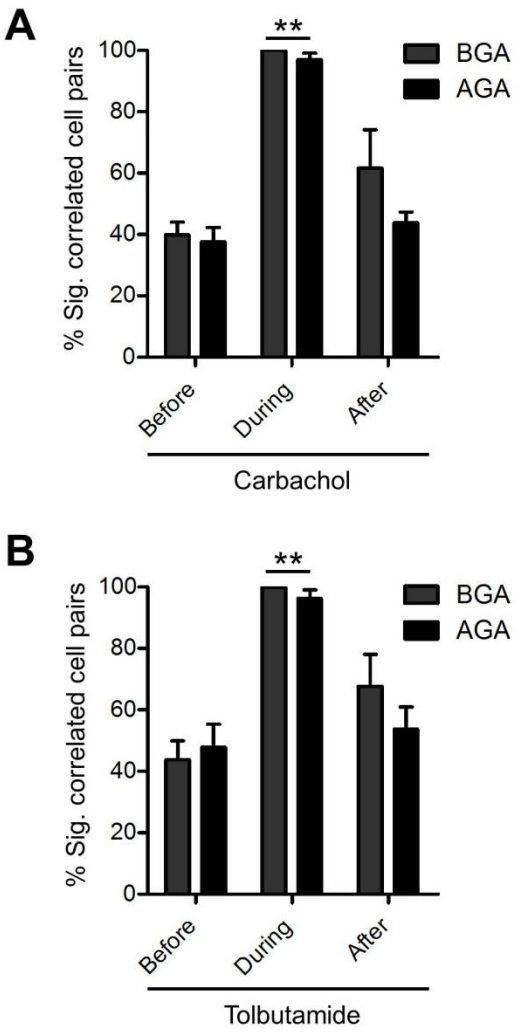

Supplemental Figure 11: Ca^{2+}-responses to carbachol and tolbutamide are unaffected by gap junction (GJ) blockade. **(A)** β-glycerrhizic (BGA; inactive analog) and 18-α glycerrhithinic acid (AGA; active analog) do not alter coordinated beta cell responses to the muscarinic agonist carbachol (10μM) (**P<0.01 *versus* before carbachol application, Kruskal-Wallis test; *n*=4 recordings). (B) As for B except following application of tolbutamide (100μM) (**P<0.01 *versus* before tolbutamide application, Kruskal-Wallis test; *n*=4 recordings). Values represent mean ± SEM.

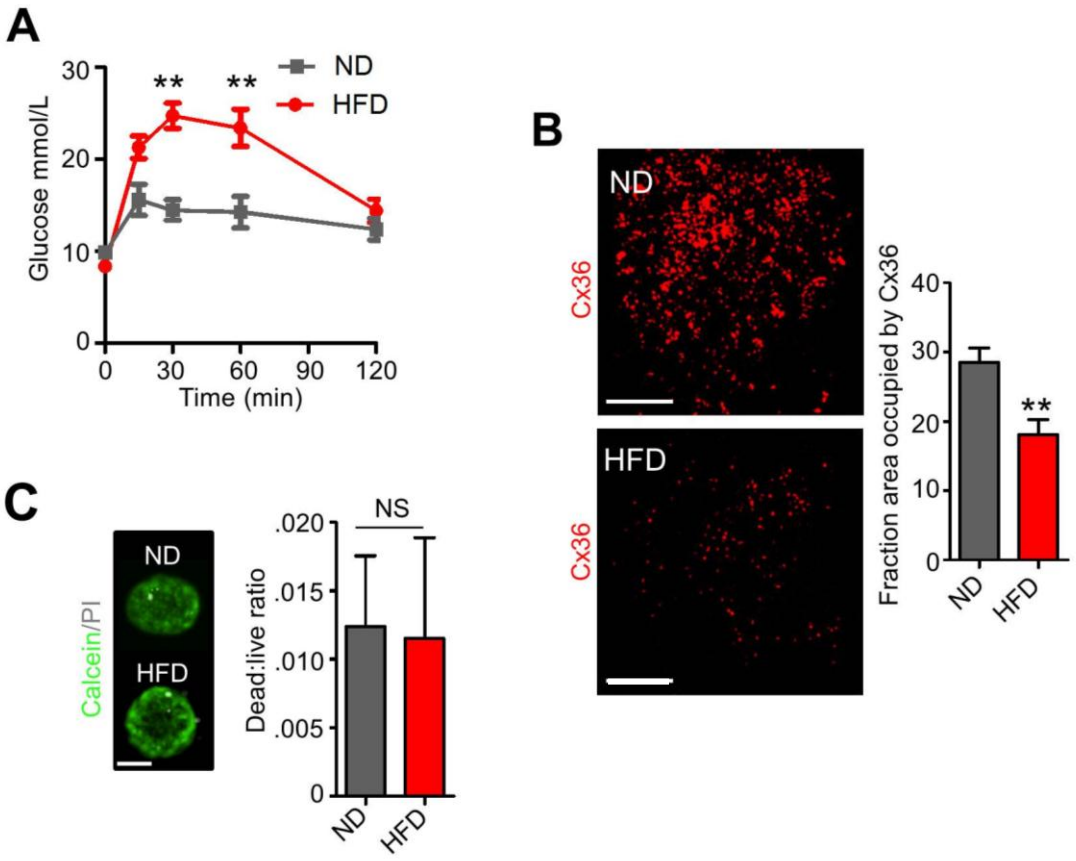

Supplemental Figure 12: Glucose tolerance, Cx36 expression and cell viability in high fat diet (HFD)-fed mice **(A)** Mice fed HFD for at least 15 weeks display glucose intolerance following intraperitoneal glucose tolerance test (IPGTT) *versus* their normal diet (ND) counterparts (**P<0.01 *versus* before; two-way ANOVA; *n*=5-10 animals). **(B)** Immunostaining of intact islets reveals a reduction in Cx36 expression in HFD-fed animals. Brightness and contrast have been linearly increased in both panels to improve visibility (scale bar = 10 µm). **(C)** HFD does not affect cell viability as assessed by the dead:live assay (*n*=6 islets from each state) (scale bar; 50 µm).

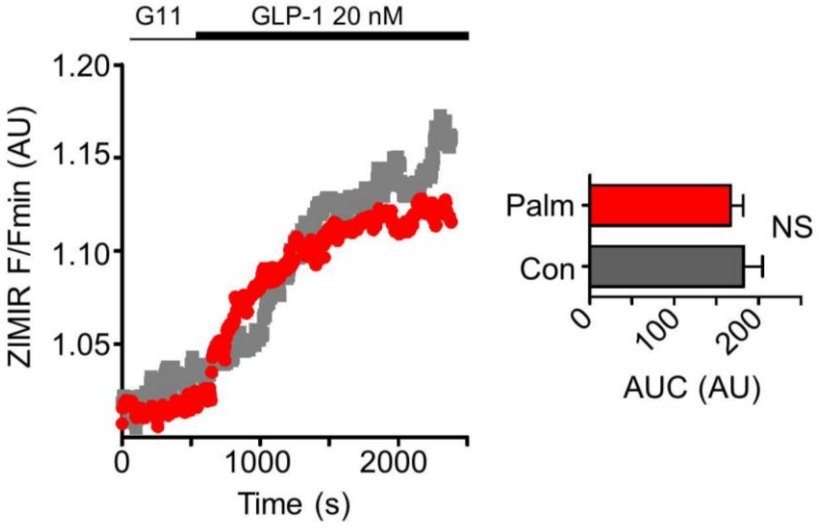

Supplemental Figure 13: Incubation of mouse islets with palmitate (Palm) does not alter the fold-change (left panel) or AUC (right panel) of GLP-stimulated insulin secretion as measured using ZIMIR (NS, non-significant *versus* control (Con); Mann-Whitney U-test; *n*=6-7 islets from 4 animals).

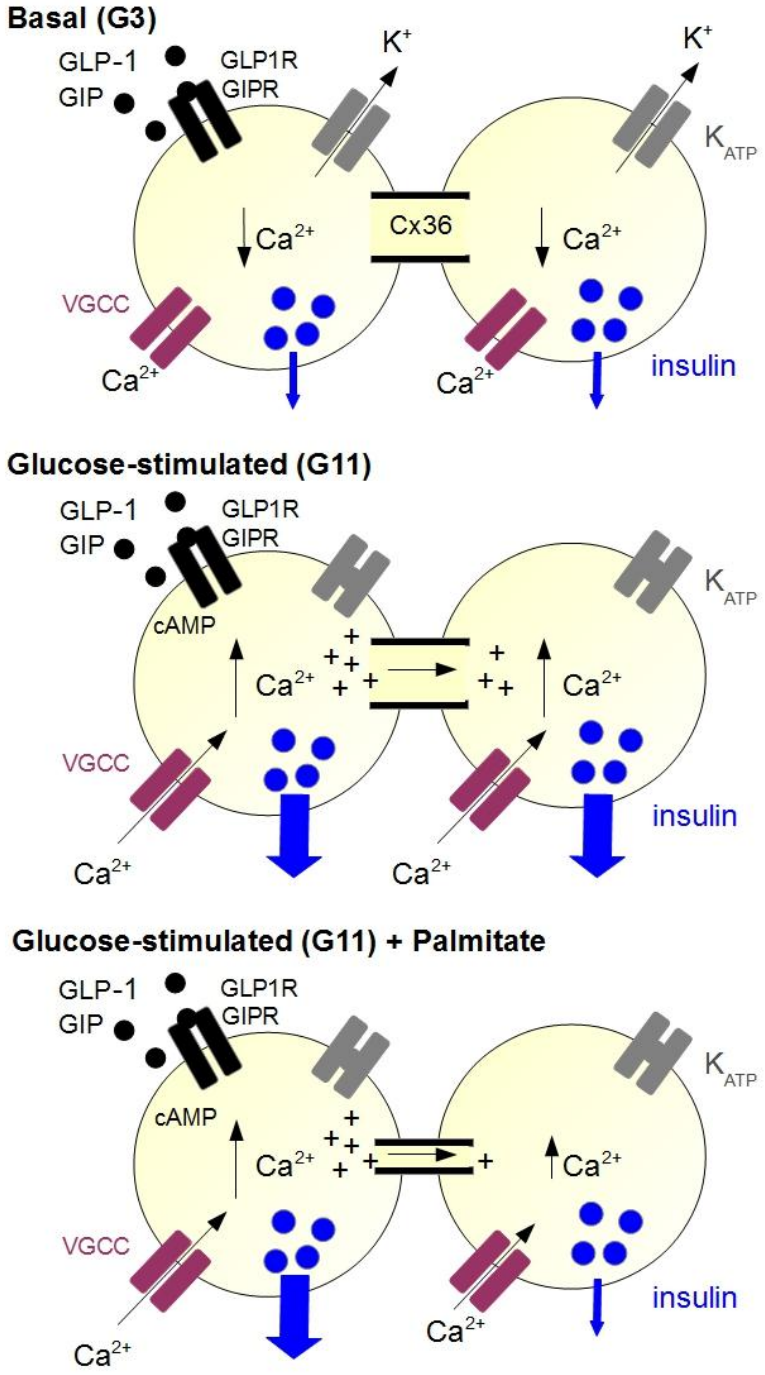

Supplemental Figure 14: Schematic depicting proposed mechanisms underlying GLP-1 and GIP effects on coordinated cell-cell activity. Under basal (normoglycemic) conditions, the incretins are unable to evoke rises in cytosolic free Ca^{2+}. At permissive glucose concentrations, K_{ATP} channels are closed and the incretins engage cAMP-dependent Ca^{2+}influx which entrains neighbouring cells via gap junctions (GJ) comprised of connexin 36. Incubation of islets with the free fatty acid (FFA) palmitate reduces GJ-signalling leading to asynchronous Ca^{2+} rises in response to GLP-1 or GIP due to impaired electrotonic coupling.

Date	Age (years)	Gender	BMI (kg/m^2)	Origin
17 May 2013	75	F	19.6	Pisa
7 May 2013	67	F	22.8	Milan
3 May 2013	52	M	24.8	Geneva
24 Apr 2013	28	F	20.2	Pisa
12 Apr 2013	51	M	30	Oxford
19 Mar 2013	51	F	41	Oxford
11 Jan 2013	67	M	27.4	Geneva
11 Dec 2012	76	F	25.4	Pisa
27 Nov 2012	68	M	27.5	Pisa
12 Nov 2012	52	M	27	Geneva
29 Oct 2012	46	M	36	Oxford
11 Oct 2012	49	M	24.1	Geneva
19 Sep 2012	79	F	29.7	Pisa
06 Sep 2012	51	M	26.2	Pisa
24 July 2012	20	M	22.8	Geneva
04 Jun 2012	43	F	34.2	Geneva
28 May 2012	80	F	27.3	Pisa
16 May 2012	50	F	20	Pisa
14 May 2012	57	F	23	Oxford
01 May 2012	46	F	26	Oxford
13 Feb 2012	56	F	19.7	Geneva

Supplemental Table 1: Summary of donor age, gender, BMI and origin.

Gene	Forward Primer	Reverse Primer
GLP1R	5' ACATCAAATGCAGACTTGCCA 3'	5' CCCAGCTCTTCCGAAATTCC 3'
UCP2	5' TAAAGGTCCGATTCCAAGCTC 3'	5' GGAGGTCATCTGTCATGAGG 3'
GJD2	5' ATCGGGAGGATCCTGTTGAC 3'	5' GAGTAGGTGATGAAGCAAAGACTG 3'
Cyclophilin (ppia)	5' AAGACTGAGTGGTTGGATGG 3'	5' ATGGTGATCTTCTTGCTGGT 3'

Supplemental Table 2: Primer sequences used for quantitative real-time polymerase chain reaction studies (qPCR).

SUPPLEMENTARY MOVIE LEGENDS

Supplemental Movie 1: Timelapse recording of calcium responses to GLP-1 in a human islet. A fluo2-loaded islet was recorded at 0.5 Hz for 50 minutes using a 491 nm laser and Yokogawa Nipkow spinning disk head to rapidly scan a large optical section without introducing lag artefacts. 11 mM glucose was continuously perfused and 20 nM GLP-1 was applied for the indicated period. Playback rate 200 frames per second (fps). Movie has been cropped to display a single islet.

Supplemental Movie 2: Timelapse recording of GLP-1-stimulated insulin release in BGA-treated islets using the Zn^{2+}-probe ZIMIR. As for Supplemental Movie 1 but islets recorded at 0.1Hz for 40 minutes in the presence of BGA.

Supplemental Movie 3: Timelapse recording of GLP-1-stimulated insulin release in AGA-treated islets using the Zn^{2+}-probe ZIMIR. As for Supplemental Movie 2 but in the presence of AGA.

Supplemental Movie 4: Timelapse recording of calcium responses to glucose and GLP-1 in a normal diet mouse islet. As for Supplemental Movie 1 but playback 60 fps to demonstrate oscillatory behaviour. Movie has been cropped to display a single islet.

Supplemental Movie 5: Timelapse recording of calcium responses to glucose and GLP-1 in a high fat diet mouse islet. As for Supplemental Movie 1 but playback 60 fps to demonstrate oscillatory behaviour. Movie has been cropped to display a single islet.